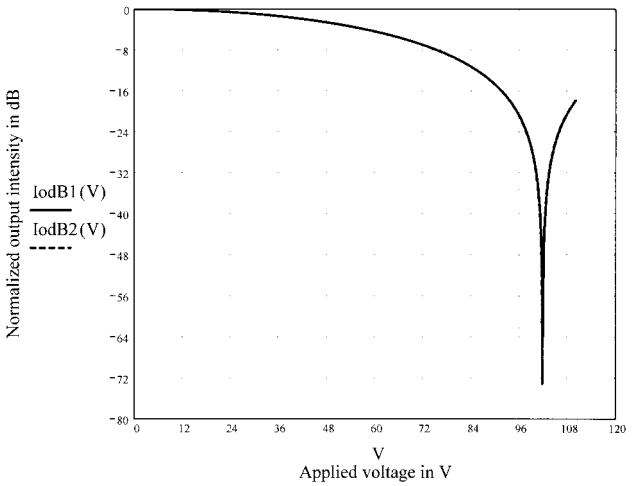

Figure 5 Plot of normalized output light intensity versus external voltage. Solid line corresponds to the result at 0°C and dashed line corresponds to the result at 65°C

electrodes, and (iii) an output collimator. To achieve optimal performance, the whole modulator, including the input collimator, sandwiched crystal module, and output collimator were carefully aligned so that an incoming light signal would be equally distributed between the pair of electro-optic crystals. In the operation, the same amounts of electric fields, but in opposite directions, were applied on two crystals. These positive and negative electric fields changed the index of refraction in opposite directions, which increased the relative phase differences between the crystals and reduced the required driving voltage. The main advantages of the presented modulator technique are: (i) polarization independence, (ii) insensitivity to ambient temperature fluctuations, and (iii) capability of handing high input power as compared with integrated optic modulators. These unique features make it possible for the modulator be widely used in optics communication networks, in which low polarization dependent loss (PDL), highly stabilized temperature performance, and high power handing capability are critically required.

REFERENCES

1. A. Yariv and P. Yeh, Optical waves in crystals, Wiley, New York, 1984.
2. Stamatios V. Kartalopoulos, Introduction to DWDM technology, IEEE Press, New York, 2000.
3. R.C. Alferness, Waveguide electro-optic modulators, IEEE Trans On Micr Theory Tech MTT-30 (1982), 1121–1137.
4. H. Nishihara, M. Haruna, and T. Suhara, Optical integrated circuits, McGraw-Hill, New York, 1989, p. 9.
5. Edward Collett, Polarized light: Fundamentals and applications, Marcel Dekker, New York, 1992.
6. www.axt.com/axt/products.htm#prodline.

FINITE-DIFFERENCE TIME-DOMAIN SIMULATION OF RESONANT MODES OF RECTANGULAR DIELECTRIC RESONATORS

Elena Semouchkina,[1] George Semouchkin,[1] Raj Mittra,[2] and Wenwu Cao[1]
[1] Materials Research Institute
Pennsylvania State University
University Park, PA 16802
[2] Department of Electrical Engineering
Pennsylvania State University
University Park, PA 16802

Received 6 August 2002

ABSTRACT: *In this paper we employ finite-difference time-domain (FDTD) simulations to study the resonant modes in rectangular dielectric resonators (DRs). Three-dimensional field patterns for these modes are derived, and the modes are represented by combinations of equivalent electric and magnetic dipoles. The possibility of exciting TM-type modes in rectangular DRs is demonstrated.* © 2003 Wiley Periodicals, Inc. Microwave Opt Technol Lett 36: 160–164, 2003; Published online in Wiley InterScience (www.interscience.wiley.com). DOI 10.1002/mop.10708

Key words: *finite-difference time-domain method (FDTD); dielectric resonators; dielectric resonator antennas; resonant modes; electromagnetic fields; mode charts*

1. INTRODUCTION

Dielectric resonator antennas (DRAs) have many desirable features, such as low cost, small size, low loss, etc., which make them suitable as devices in millimeter wave applications [1]. The resonant modes in cylindrical and hemispherical DRAs, which are bodies of revolution and amenable to convenient analysis by using the integral methods, have been studied extensively in the past; in particular, the TE, TM, and hybrid types of modes in these antennas have been investigated. However, there is little information available in the literature about the resonant modes in rectangular DRAs, although the latter are often preferred over the cylindrical and hemispherical DRAs, because they are easier to fabricate and offer more degrees of freedom to control the resonant frequency and the quality factor [2]. The modal analysis [2] of the rectangular DRAs has been limited to a few TE modes.

The finite-difference time-domain (FDTD) method employs a Cartesian grid and is well suited for modeling rectangular objects of the type investigated in this paper. In a previous work, we have employed the frequency-domain representation of the time-domain data simulated via the FDTD method to study the 2D resonant

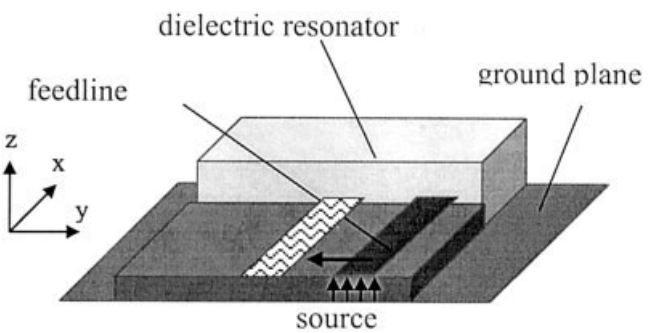

Figure 1 Schematic of DRA excitation

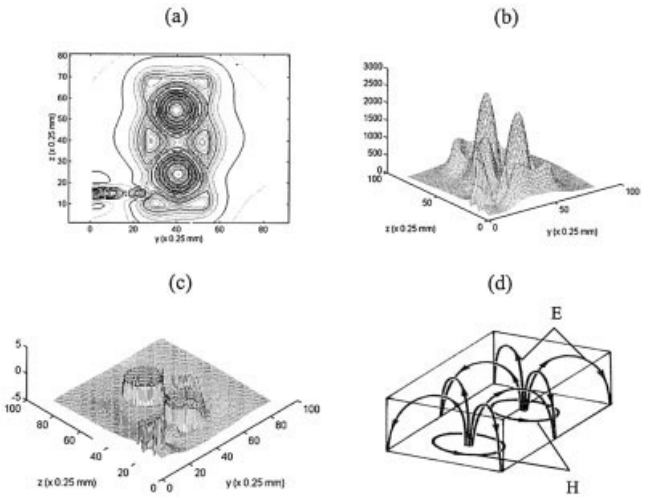

Figure 2 (a) Contour plot; (b) 3D plot; (c) phase plot of the normal electric field component of the TM_{241} mode (7.2 GHz) in the DRA with dimensions of 5.6 × 12 × 1.8 mm in the plane located 0.5 mm above the ground plane; (d) mode chart of the TM_{241} mode

modes in microstrip and patch antenna structures [3]. Later, we extended this technique to investigate the 3D resonant modes of DRAs [4]. In the present work we continue our efforts to analyze the resonant modes of rectangular DRAs by using the FDTD method, and to investigate the effects of the DRA's dimensions and its surface metalization, and the feed location on the formation of the resonant modes.

2. SIMULATION PROCEDURE

We have modeled a variety of DR antennas, all of which have a dielectric constant of 88. However, they have different dimensions and different types of surface metalization, such as metal strips on the faces of the dielectric block or on the sides. The resonators are assumed to be located on an infinite ground plane, which serves as one of the boundaries of the computational domain, while perfectly matched layers (PML) are placed at all other boundaries. The resonator is excited by a microstrip transmission line, which is terminated at the side surface of the resonator. We have investigated different locations of the microstrip by shifting it along the length of the dielectric block, as shown in Figure 1. An electric field source of Gaussian type with a bandwidth of 12 GHz modulated by a sinusoidal wave of 6 GHz was employed to excite the microstrip line.

TABLE 1 Dipole Representation of the Modes in the DRA with the Dimensions of 3 × 12 × 1.8 mm

Frequency	6.2 GHz	7.0 GHz	7.6 GHz
Field schemes	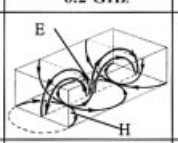	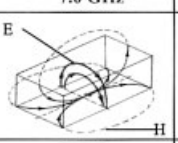	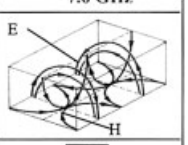
Dipole locations	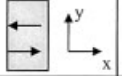		
Mode types	TE^{x}_{121}	TE^{y}_{111}	TE^{y}_{121}
Radiation ability	Nonradiating	Radiating	Nonradiating

TABLE 2 Elimination of Resonant Modes in the DRA with Dimensions of 3 × 12 × 1.8 mm by Changing the Feed Location

Frequency (GHz)	6.2	7.0	7.15	7.6	7.9	8.4
Mode type	TE^{x}_{121}	TE^{y}_{111}	TE^{x}_{131}	TE^{y}_{121}	TE^{x}_{141}	TE^{y}_{131}
Dipoles' Locations / Feed type			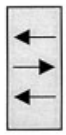			
Asymmetric Feed	yes	yes	yes	yes	yes	yes
Symmetric Feed	yes	yes	no	no	yes	yes

The time-domain simulations are used to model the distributions of electric- and magnetic-field components inside the DRAs, and the fast Fourier transform (FFT) is subsequently applied to derive the corresponding amplitude and phase distributions at different frequencies. The input return loss spectra have also been simulated in order to determine the resonant frequencies. The analyses of the resonant amplitude and phase distributions have enabled us to plot the 3D charts of the resonant modes, and to describe them as combinations of magnetic or electric dipoles located within the DRA. This type of equivalent dipole representation is useful for predicting the radiation efficiency and directivity of the DR antennas at different resonant frequencies.

3. RESONANT MODE ANALYSIS

Figure 2 presents an example of the analysis of the resonant mode excited at 7.2 GHz in the DR, whose dimensions are 5.6 × 12 × 1.8 mm. The contour plot and the 3D distribution of the amplitude of the normal electric field component, as well as its phase distribution in the plane located between the ground plane and the upper surface of the dielectric block, are depicted in Figures 2(a)–(d), respectively. We also have simulated the distributions of all other field components of the DR at different cross sections. The obtained data enabled us to construct the 3D field chart of the mode, which is depicted in Figure 2(d). The observed mode is of TM_{241} type and its fields are similar to the ones produced by two vertical

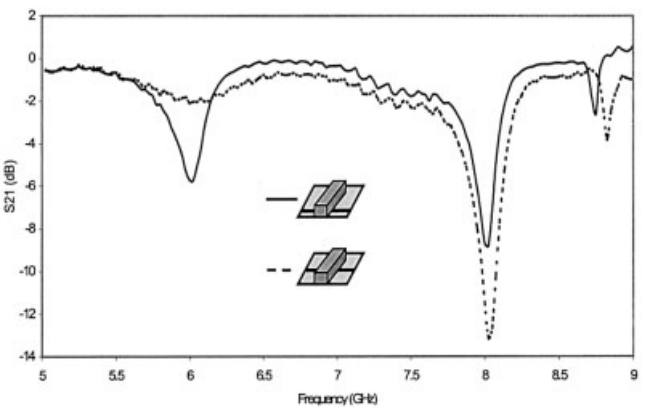

Figure 3 Experimentally measured $|S_{21}|$ spectra of the DRAs with different feed locations: asymmetric feed (solid curve) and symmetric feed (dashed curve). Geometry of excitation is shown in the inset

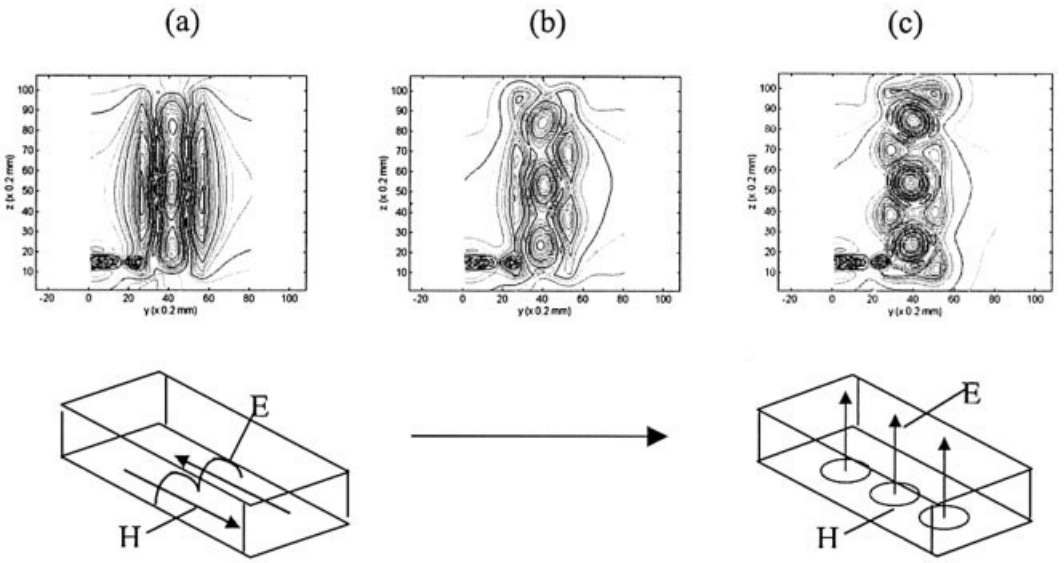

Figure 4 Contour plots of the normal electric field component illustrating mode transformation in the DRAs with length of 18 mm, height of 1.8 mm, and different widths: (a) 6.2 mm; (b) 5.6 mm; (c) 5.3 mm. TE_{211} mode (two horizontal magnetic dipoles) is transformed into the TM_{261} mode (three vertical electric dipoles)

electric dipoles. The conditions for exciting the TM-type modes in the rectangular DRAs will be discussed later in this section.

Table 1 shows the resonant frequencies, the 3D field charts, and their dipole representations for the three modes excited in a DRA with dimensions of $3 \times 12 \times 1.8$ mm. As seen from the table, only the TE^{y}_{111} mode is expected to be efficiently radiating, since the other two modes are both equivalent to two oppositely-directed dipoles.

One of the advantages of using the FDTD method for the modal analysis is that it is able to reproduce the real environment of the resonant structure, particularly the type of excitation and location of the feed. Table 2 presents the characteristics of the resonant modes produced by a DRA with dimensions of $3 \times 12 \times 1.8$ mm, and the corresponding combinations of the magnetic dipoles for the cases of two different locations of the microstrip feedline, which are depicted in Figure 1. We excite a higher number of modes with asymmetric locations of the feedline, while symmetric feeds serve to suppress some of the resonant modes, and this effect is similar to the one observed in microstrip patch structures [5]. The feed point produces an electric wall type of environment and this, in turn, prevents the modes that do not satisfy this condition from getting excited. The understanding of this phenomenon is useful for selective elimination of certain resonant modes in the DRA.

Experimentally measured insertion loss spectra of the DRA for symmetric and asymmetric feed locations, shown in Figure 3, validate the resonant mode elimination concept for symmetric feeds. The geometry of the DRA excitation in these measurements is shown in the inset of the figure. The DRA was placed on top of microstrip line and then shifted with respect to the microstrip for this configuration.

It was found in our study that the variation of antenna dimensions strongly influenced resonant mode formation in the rectangular DRAs. We have observed that increasing the DRA height causes a decrease in the resonant frequency of the mode without altering the nature of the mode. For example, changing the height from 1.8 mm to 3.6 mm causes a decrease of the resonant frequencies by ~1 GHz, and this effect can be very useful for tuning the frequency of the desirable modes in a DRA. In addition, it was found that an increase of the DRA height also causes a weakening of some of the modes.

Increasing the DRA width not only decreases the resonant frequencies, but also causes additional new modes to appear. Figure 4 demonstrates the mode transformation in the DRAs with length of 18 mm and height of 1.8 mm, but with slightly different widths, namely, 6.2 mm, 5.6 mm, and 5.3 mm, respectively. It is seen from this figure that decrease of the DRA width transforms the TE_{211} mode, which corresponds to two horizontal, oppositely-

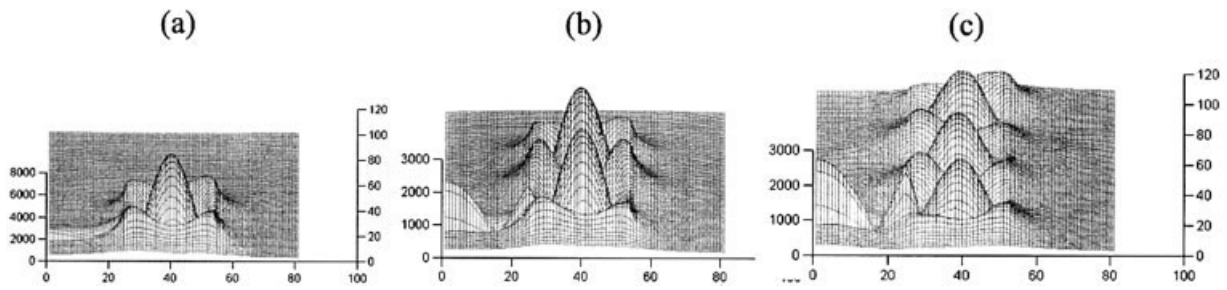

Figure 5 Array-type of modes excited in the DRAs with dimensions of: (a) $1.8 \times 5.6 \times 5.6$ mm—TM_{221} mode; (b) $1.8 \times 5.6 \times 12$ mm—TM_{241} mode; and (c) $1.8 \times 5.3 \times 18$ mm—TM_{261} mode

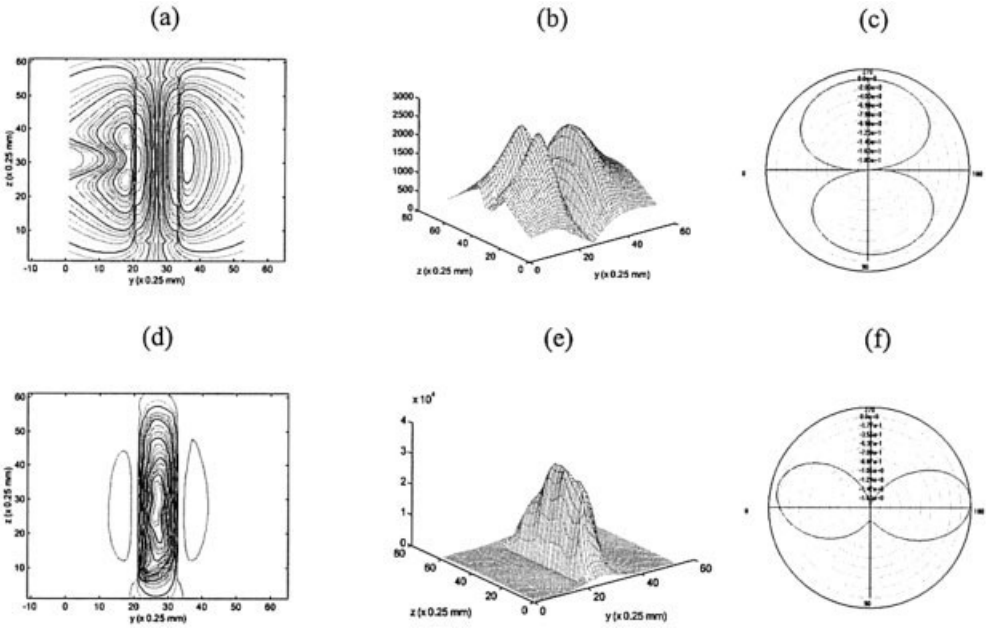

Figure 6 (a, d) Electric field contour plots; (b, e) 3D field distributions; (c, f) radiation patterns of DRAs with dimensions of 3 × 12 × 1.8 mm at 7 GHz: (a–c) TE_{111} mode (horizontal magnetic dipole) in DR antenna without metal strips; and (d–f) TM_{111} mode (vertical electric dipole) in DR antenna with metal side strips

oriented magnetic dipoles, into the TM_{261} mode, which corresponds to three vertical electric dipoles.

The simplest mode of the same type as the TM_{261}, the TM_{221} mode, was found to exist in antennas with dimensions of 5.6 × 5.6 × 1.8 mm (Fig. 5(a)), while the TM_{241} mode was excited in the DRA with dimensions of 5.6 × 12 × 1.8 mm. All of the modes depicted in Figure 5 have been observed to appear at approximately the same frequency and the only difference between them was the number of electric dipoles placed along the antenna length. An analysis of the phase distributions of this type of modes has shown that the fields of the electric dipoles have the same phases (see Fig. 2(c)). This implies that the observed TM modes could be used to create arrays of electric dipoles.

Our data show that the formation of the TM modes in the rectangular DRAs, described above, is possible only if the antenna dimensions provide sufficient "space" to host each of the dipoles. For the case of only one dipole, the shape of the horizontal cross-section of the DRA should be close to a square, while the additional row of dipoles could be excited in longer rectangular antennas.

We also have studied the effect of surface metalization on the resonant modes in the DRA. It was found that thin metal strips on front faces of the DRA cause an increase of the resonant mode frequency, while the side face metalizations eliminate a number of modes, stimulating, instead, the formation of only one type of modes, namely, the cavity-type modes. Figure 6 demonstrates the effect of metallic strips placed on the sides of a DRA with dimensions of 3 × 12 × 1.8 mm, in which we observed only the TE-type modes in the absence of the metalization. As seen from the above figure, in the DR antenna without metallic strips, the TE_{111} mode that corresponds to a horizontal magnetic dipole, is observed at the frequency of 7 GHz, while the TM_{111} mode, which corresponds to the vertical electric dipole, is observed at the same frequency in the DR antenna with metal side strips. The radiation patterns for these two modes shown in Figure 6(c) and (f) have different directivity. The possibility of exciting TM modes in rectangular DR antennas appears to be very attractive, because these modes, in contrast to the TE_{111} mode radiating toward the zenith, have a beam maximum along the azimuth plane instead. The latter is often desirable in communication applications.

3. CONCLUSION

We have demonstrated that the FDTD method is very efficient for studying resonant modes in rectangular DR antennas. Standing wave patterns of electric and magnetic field components were simulated and the 3D patterns for different mode types were generated. It was shown that the resonant fields in rectangular DRAs could be represented by combinations of magnetic or electric dipoles located within the DRs. The dimensions of the DRs were found to be critical for the excitation of the different mode types. The effects of DRA dimensions, feed location, and surface metalization on the mode formation were investigated. The possibility of exciting TM modes in rectangular DRAs, particularly the modes equivalent to arrays of vertical electric dipoles, was demonstrated.

ACKNOWLEDGEMENT

This work was supported by the National Science Foundation, as part of the Center for Dielectric Studies under grant no. 0120812.

REFERENCES

1. R.K. Mongia and P. Bhartia, Dielectric resonator antennas-A review and general design relations for resonant frequency and bandwidth, Int J Microwave Millimeter-Wave Eng 4 (1994), 230–247.
2. R.K. Mongia and A. Ittipiboon, Theoretical and experimental investigations of rectangular dielectric resonator antennas, IEEE Trans Antennas Propagat 45 (1997), 1348–1356.
3. E. Semouchkina, W. Cao, R. Mittra, and W. Yu, Efficient determination of resonant frequencies in resonant structures using the FDTD method, Microwave Optical Tech Lett 28 (2001), 244–247.

4. E. Semouchkina, G. Semouchkin, W. Cao, and R. Mittra, FDTD analysis of modal characteristics of dielectric resonator antennas, IEEE AP-S Dig Proc Int Symp, San Antonio, 2002, pp. 466–469.
5. E. Semouchkina, W. Cao, R. Mittra, and M. Lanagan, Effect of feeding symmetry on resonance in patch and capacitor structures, IEEE AP-S Dig Proc Int Symp, Boston, 2001, pp. 486–489.

L-BAND 360° BROAD-BANDWIDTH MONOLITHIC ANALOG PHASE SHIFTER

K. Liu,[1] E. Y. B. Pun,[1] and X. J. Tian[2]
[1] Department of Electronic Engineering
City University of Hong Kong
83 Tat Chee Avenue Kowloon Tong
Kowloon, Hong Kong
[2] Department of Electronic Engineering
JiLin University
ChangChun, No. 119 Road
P.R. China

Received 8 July 2002

ABSTRACT: *An L-band 360° broad-bandwidth analog phase shifter is designed using varactor. New design equations for expanding bandwidth and improving linear phase-shift are derived and applied to performances optimization in one circuit. The analog phase shifter is fabricated using MIC and SMT technologies. At 1.2 ~ 2.0 GHz (L-band), total phase-shift of 360° and linear deviation of less than ±2.5% were obtained, and the insertion loss varied less than 2 dB across the band.* © 2003 Wiley Periodicals, Inc. Microwave Opt Technol Lett 36: 164–166, 2003; Published online in Wiley InterScience (www.interscience.wiley.com). DOI 10.1002/mop.10709

Key words: *analog phase shifters; broad bandwidth; varactor diodes; microwave circuits*

INTRODUCTION

Analog phase shifters find uses in a number of applications that require continuous linear phase control of RF/microwave carrier signals. Examples of such applications include phased-array radar, heavy ion accelerators, microwave communications, and so on. The L-band 360° phase shifter described here can be applied in microwave phase-shift scanning of an electronic-optic sampling system [1].

Previously reported analog phase shifters operate mostly in the 3-GHz to 18-GHz frequency range [2–4]. There have been few reports on 360° analog phase shifters operating at the L band (1 ~ 2 GHz). An analog phase shifter for adaptive antennas at 1 GHz has been reported, but it has only 90° phase shift [5].

The ideal electrical control phase shifter should have the following properties: (i) 360° phase shift, (ii) broad bandwidth, (iii) linear phase shift, and (iv) constant insertion loss. Many efforts have been made to solve above problems, but no effort has been made to solve all properties in one circuit. Conventional analog phase shifter generally uses reflection-type structure [4], which minimizes the number of diodes, as only one diode per 180° phase shift network is required. The reflection-type phase shifter produces the phase shift by reflecting the incident wave with a varactor whose capacitance varies according to the bias voltage. In this paper, an optimal design of the reflection-type phase shifter structure is presented and bandwidth design equations are deduced. The three performances: 360° phase shift, broad bandwidth, and linear phase shift were studied in one circuit. We found that the selection of a varactor diode directly affects performances of the phase shifter, and circuit optimization design also decreases the phase shifter's insertion loss.

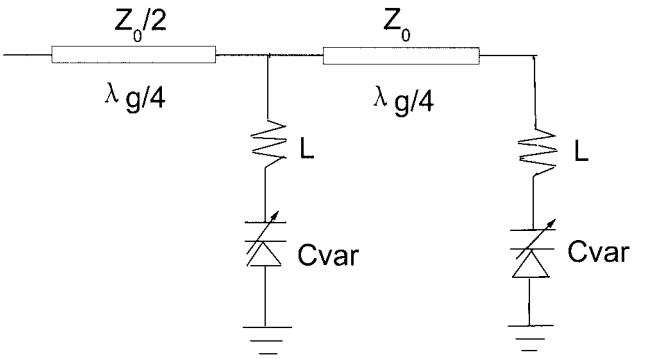

Figure 1 Dual varactor termination for 360° phase shift

BROAD-BANDWIDTH DESIGN

Figure 1 shows that the reflection termination composed of two varactors connected in parallel with $\lambda_g/4$ transmission line length can achieve 360° phase shift [4]. Broad-band application of an analog phase shifter is to make phase shifter maintaining 360° phase shift, high linearity (linear voltage-phase relationship), and constant insertion loss at the broadest frequency range. In this work, the bandwidth design equations against phase-shift error, varactor gamma value, and relative bandwidth will be derived.

The phase shifter's termination reactance curve $A_o - B_o V_n^r$ must closely match the tangent curve $-\tan(kV_n + \varphi_o)$ when working at centre frequency ω_o, the linear phase shift can be obtained. This relationship is written as [6]:

$$A_o - B_o V_n^r \approx -\tan(kV_n + \varphi_o) \tag{1}$$

and

$$A_o = \omega_o L/Z_o,\ B_o = 1/(\omega_o C_{\min} Z_o),\ V_n = (V - V_\phi)/(V_{\max} - V_\phi), \tag{2}$$

where A_o and B_o are the design parameters at ω_o. V_n, γ, and φ_o are the normalized biased voltage of varactor, varactor gamma value, and initial phase angle, respectively, and k is the proportional constant, $C_{\min}$ is the minimum capacitance, and V_ϕ is the contact potential. Since A_o and B_o are functions of frequency, Eq. (1) will not be satisfied when the frequency deviating from ω_o. If the phase shifter still requires a 360° phase shift, the varactor's reactance curve $A - BV_n^r$ with deviated ω_o must match another tangent curve. Thus, after selecting the most suitable A_o, B_o, and γ, every reactance curve $A - BV_n^r$ has a corresponding tangent curve to match, and we can obtain broadband application while ensuring linear phase shift. The reactance curve with deviated ω_o is $A - BV_n^r$, then give using Eq. (2):

$$A = \omega L/Z_o = A_o(\omega/\omega_o),\ B = 1/(\omega C_{\min} Z_o) = B_o/(\omega/\omega_o), \tag{3}$$

where ω is the optional frequency deviating ω_o. We can define $\omega/\omega_o = \alpha$, thus $A = A_o\alpha$, $B = B_o/\alpha$, and Eq. (1) becomes

$$A - BV_n^r = A_o\alpha - (B_o/\alpha)\cdot V_n^r \approx -\tan(kV_n + \varphi_o). \tag{4}$$